

Article

Research on the Permeability and Pore Structure Distribution Characteristics of High-Performance Mortar for Surface Treatment of Bridge Piers and Columns

Xianzheng Yu ¹, Hua Liu ², Xiaolin Fan ¹, Liangyu Zhu ¹, Chengqi Zhang ¹ and Shiyi Zhang ^{3,*}

¹ China Railway Bridge and Tunnel Technology Co., Ltd., Nanjing 210000, China; yuxianzheng1986@163.com (X.Y.); jerry05071986@126.com (X.F.); zly724026@163.com (L.Z.); lzjtzcq@163.com (C.Z.)

² China Railway Major Bridge Reconnaissance & Design Institute Co., Ltd., Wuhan 430000, China; kylinbridge@163.com

³ School of Civil Engineering and Geomatics, Shandong University of Technology, Zibo 255000, China

* Correspondence: zhangsy986@163.com

Abstract: In marine environments, bridge piers and columns are prone to corrosion caused by harmful media, particularly chloride ions. This corrosion can lead to cracking of the steel bars in the protective layer of the bridge piers. To enhance the corrosion resistance of concrete in bridge piers, this article introduces the use of nanoclay-modified cement mortar. This innovative material offers high-performance surface treatment options that can effectively slow down the erosion process of harmful media and reduce the risk of bridge pier column cracking. To evaluate the ion erosion resistance of this nanoclay-modified cement mortar, we conducted detailed experiments on the pore structure of cement paste. The pore structure of cement paste with different dosages of nano-kaolinite clay and the dispersion method was studied using mercury intrusion porosimetry (MIP). The fractal dimension of the pore surface area of the net cement paste was calculated from the fractal model based on thermodynamic relationships of the pore structure-related parameters obtained with mercury pressure experiments. The relationship among the multiple fractal dimensions, pore structure parameters, dispersion mode, and permeability is explored. The results show that the addition of nano-kaolinite clay particles can improve the internal pore structure of cement materials. When 1.5% nano-kaolinite clay is mechanical dispersed, the total specific pore volume and the most probable pore size are reduced by 47.83% and 56.87%, respectively, compared with the control group. The fractal dimension image of cement-based materials with nano-kaolinite clay has a range of singular points and does not have fractal characteristics in this range. Nano-kaolinite clay has a significant effect on the fractal dimension of pore size range I. The fractal dimension of the whole pore size range is not suitable for the analysis of permeability, and the fractal dimension calculated by selecting less than the critical pore size range has a good correlation with permeability.

Keywords: multifractal; nano-kaolinite clay; pore structure; permeability; decentralized approach



Citation: Yu, X.; Liu, H.; Fan, X.; Zhu, L.; Zhang, C.; Zhang, S. Research on the Permeability and Pore Structure Distribution Characteristics of High-Performance Mortar for Surface Treatment of Bridge Piers and Columns. *Buildings* **2024**, *14*, 811. <https://doi.org/10.3390/buildings14030811>

Academic Editor:
Abderrahim Boudenne

Received: 21 February 2024

Revised: 11 March 2024

Accepted: 14 March 2024

Published: 16 March 2024



Copyright: © 2024 by the authors. Licensee MDPI, Basel, Switzerland. This article is an open access article distributed under the terms and conditions of the Creative Commons Attribution (CC BY) license (<https://creativecommons.org/licenses/by/4.0/>).

1. Introduction

In recent years, with economic growth, the number of structures in marine environments has been steadily increasing. Concrete structures constitute the majority of these. However, the harsh marine environment poses significant challenges to the durability of these concrete structures. During its service life, concrete is constantly exposed to various loads, environmental factors, and their combinations, especially chloride ion penetration-induced steel corrosion, which negatively impacts the service performance and durability of concrete. Concrete is intrinsically a porous material, and its durability largely depends on its permeability, which is determined by the pore structure within it [1–3]. Improving the durability of concrete materials is a crucial technical prerequisite for ensuring the longevity

of infrastructure. When compared to traditional mineral admixtures, nanomaterials offer significant advantages. Many researchers have confirmed that even at a very small percentage, nanomaterials can enhance the strength of cement composites, and the microstructure becomes denser, ultimately improving the durability of concrete [4–6]. Nanoclay materials have recently emerged as a highly researched field within the civil engineering and construction industries [7]. The development of nanomaterials has not only improved the performance and durability of existing materials but has also propelled the evolution of concrete materials towards multifunctionality and high performance.

As a new nanomaterial, nano-kaolinite clay (NKC) has been developed and applied in concrete in recent years [8]. Nano-kaolinite clay is the powder kaolin clay refined from the kaolin raw ore after crushing with a crusher followed by ultrafine crushing with an impact mill, calcination, airflow ultrafine crushing, and other processes. Moreover, its low price makes it easy to apply in practical engineering. Compared to other nanomaterials (e.g., nano-SiO₂, nano-CaCO₃, etc.), NKC is more suitable for concrete modification [9]. Nano-kaolinite clay particles fill the nanopores of cement paste. The addition of nano-fine particles can improve the properties of concrete by increasing the surface area and reactivity [10], significantly improve the microscopic density [10], and improve the resistance to chloride ion penetration [11]. The filling effect of NKC [12], volcanic ash activity [13], and nucleation reduce the number of pores in concrete [14,15]. It also improves resistance to the aggressive effects of chloride ions and the diffusion of harmful ions [16]. M. S. Morsy et al. [17] reported that the matrix structure becomes denser when NMC is added up to 7.5%, and the pore structure becomes larger when the concentration is higher. Mahyuddin B. Ramli et al. [18], in their study on the early mechanical strength of cementitious composites, showed that 10% metakaolin replacement of cement increased the compressive strength of concrete. Liu Kangning et al. [9] concluded that the internal pores of recycled concrete with a metakaolin replacement rate of 15% were significantly reduced, and a large amount of hydrated calcium silicate gel was generated inside the recycled concrete, which had the best adhesion to fibers.

When studying the relationship between the macroscopic properties of concrete and its pore structure, it is more challenging to study the relationship because the pore structure of concrete is highly complex, and there are no rules. In 1985 Winslow [19] applied fractal theory to concrete, which allows complex disordered features to be quantitatively characterized as fractal dimensions. Shanshan Jin et al. [20] found a close relationship between the fractal dimension of the pore surface area and the pore structure parameters as well as the strength of the mortar. Han Xiao et al. [21] showed that the relationship between fractal dimension and mean aperture, median aperture, most feasible aperture, and threshold aperture follows the exponential function with the highest correlation, while the relationship between fractal dimension and porosity, pore area, and pore volume is more in line with the quadratic polynomial function. Han Xiao et al. [22] showed that the fractal dimension can clearly describe the internal pore characteristics and has a good correlation with the most probable pore size and the specific surface area of the pore.

In the study of seawater-mixed cement slurries by Qi et al. [23], it was shown that pore structures with different size ranges can have different fractal dimensions in a size-dependent manner. This fractal feature is known as a multifractal. Multiple fractal analysis, as an advanced fractal theory, has been applied in recent years to study the pore structure of cementitious composites. Its main working principle is to characterize the pore structure of materials by describing the complexity and spatial validity of the geometries [24]. Valentini et al., used multiple fractals obtained from digital images of cement pastes as a structural probe to quantify the tendency of clusters to be formed by hydrated calcium silicate (C-S-H) gels [25]. Multiple fractal features have also been identified by several researchers, including Winslow [19] and Valentini [26], through their studies of cement paste pore structures. Compared with the traditional single fractal model, the multifractal model can characterize the pore structure of cement paste with local singularities and size dependence more scientifically and reasonably [25]. Liu Yao et al. [27] showed that with the increase in curing age or the ratio of lime to sand, the fractal dimension (D) of the distribution of small pore

diameter of concrete pore structure generally increased. In contrast, the fractal dimension (D) of the distribution of large pore diameter and permeability generally decreased. In recent years, studies related to the characterization of porous media using multifractal dimensions have been rapidly developed [28]. It is well known that multifractal analysis provides a new characterization of disordered porous media in terms of local singularity and scale dependence. Therefore, combining the pore structure test with fractal theory can obtain the pore structure information of concrete from multiple dimensions and then establish the relationship between microstructure and macroscopic properties. Applying the concept of multiple fractals to the characterization of the pore structure of cement paste is beneficial for evaluating the durability of concrete structures. In addition, the accuracy of the results is reduced when calculating the fractal dimension of the entire pore region [29]. Therefore, when studying the multifractal characteristics of the pore structure of cement-based materials and the relationship between their permeability, selecting a suitable multifractal model can help us better understand the properties and mechanism of nano-kaolinite clay cement-based materials.

In the existing literature, there are few studies on the fractal dimension of the pore structure of cement-based materials with mineral admixtures, such as nano-kaolinite clay, and few discussions on the selection of appropriate models for different pore size ranges in the study of fractal dimension. Based on the above, in this paper, the pore structure of cementitious materials was tested mainly using the mercury intrusion pressure (MIP) method to reveal the modification mechanism of nano-kaolinite clay particles on the properties of cementitious materials from a microscopic perspective. In this paper, the fractal dimension of the pore surface area is derived and calculated for cementitious materials. On this basis, the multiple fractal characteristics of the pore structure of cementitious materials with different doses of nano-kaolinite clay and the relationship with their permeability and dispersion mode are discussed.

2. Materials and Methods

2.1. Raw Materials

The water used for the test was tap water. The cement is Shanshui PO42.5R ordinary silicate cement. The chemical composition is detailed in Table 1. The morphology of cement is shown in Figure 1. The specific surface area of cement is 400 m²/Kg.

Table 1. Chemical composition of cement.

| Chemical Composition | CaO | SiO ₂ | Al ₂ O ₃ | Fe ₂ O ₃ | MgO | SO ₃ |
|----------------------|-------|------------------|--------------------------------|--------------------------------|------|-----------------|
| Content/% | 59.31 | 21.90 | 6.26 | 3.79 | 1.63 | 2.41 |

The nanoparticle material chosen for this experiment was nano-kaolinite clay nanoparticles. It is the raw kaolin ore after coarse and medium crushing with a crusher. The material is then subject to ultra-fine grinding using an impact mill and refined using calcination (the calcination temperature is 750 °C–900 °C). The chemical composition and main technical parameters are listed in Tables 2 and 3, respectively. The microstructure and XRD images are shown in Figure 2.

Table 2. Chemical composition of nano-kaolinite clay.

| Chemical Composition | CaO | SiO ₂ | Al ₂ O ₃ | Fe ₂ O ₃ | MgO | K ₂ O | TiO ₂ | Na ₂ O |
|----------------------|------|------------------|--------------------------------|--------------------------------|------|------------------|------------------|-------------------|
| Content/% | 0.28 | 47.80 | 41.80 | 0.30 | 0.03 | 0.58 | 0.02 | 0.06 |

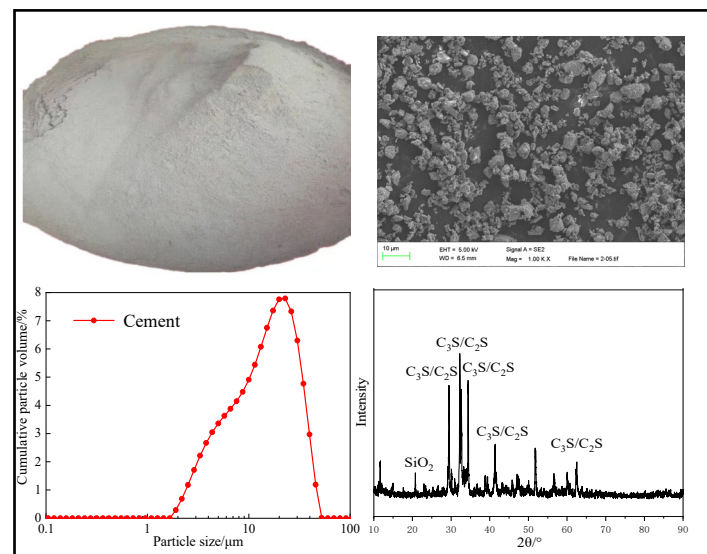


Figure 1. Cement morphology.

Table 3. Main technical indexes of nano-kaolinite clay.

| Parameter | Mean Diameter/mm | Relative Density/g/cm ³ | PH |
|------------------|------------------|------------------------------------|-----|
| Technology index | 370 | 2.58 | 7.9 |

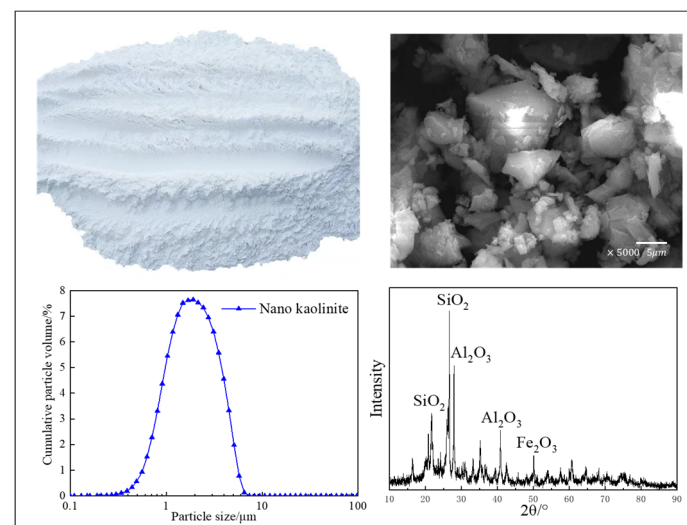


Figure 2. Morphology of nano-kaolinite clay.

2.2. Sample Preparation and Mix Ratio

To investigate nano-kaolinite clay nanoparticles' effect on cementitious materials' pore structure, the effect of the dispersion mode of the kaolin clay nanoparticles was first investigated. In the experiments, the nano-kaolinite clay was dosed at 0%, 0.75%, 1.0%, and 1.5%, separately, in cement-based specimens with a fixed water/cement ratio W/B of 0.5. The dispersion method was both manual and mechanical. The nano-kaolinite clay was evenly dispersed in water and mixed with cement using a cement net mixer to form a slurry, which was poured into a 40 mm × 40 mm × 160 mm test mold and vibrated 60 times. The cast specimens are cured in a standard curing chamber (temperature 20 ± 1 °C, relative humidity $\geq 95\%$) for 24 h. After demolding, the molds remain in standard conditioning chambers until the specified age. The sample preparation flow chart is shown in Figure 3. The specimen numbers are shown in Table 4. Mercury intrusion porosimetry (MIP) was completed for the cement specimens, and the results are shown in Table 4.

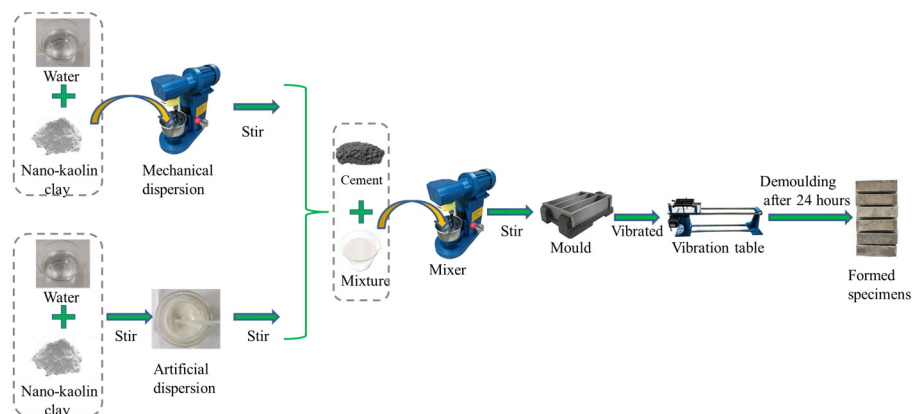


Figure 3. Flow chart of sample preparation.

Table 4. Cement samples under different dispersed methods.

| Sample | Nano-Kaolinite Clay Content/% | Dispersion Mode | Dispersion Time/min |
|--------|-------------------------------|-----------------|---------------------|
| NC0 | 0.00 | - | |
| NCH1 | 0.75 | Artificial | 3 |
| NCH2 | 1.00 | | |
| NCH3 | 1.50 | | |
| NCM1 | 0.75 | Machinery | |
| NCM2 | 1.00 | | |
| NCM3 | 1.50 | | |

2.3. Experimental Methods

2.3.1. Mercury Intrusion Porosimetry (MIP)

Aperture size, pore size distribution, and coherence between pores are the main factors affecting cementitious materials' chloride ion permeation properties. The chloride permeation performance of cementitious materials is mainly influenced by the following factors: aperture size, pore size distribution, coherence between pores, the chemical composition of the cementitious material, and age of care. Nano-kaolinite clay particles can fill microscopic pores and cracks in concrete and improve the compactness of cementitious materials, thus affecting their physical and mechanical properties. Also, to reveal these properties of nano-modified cementitious materials, the effect of nano-kaolinite clay particles on the pore structure of cementitious materials needs to be observed and analyzed at a microscopic level. Three standard methods are used for testing the pore structure properties of cementitious materials. These include the water vapor adsorption test method, the nitrogen adsorption test method, and MIP. The development law of cement-based pore structure of nano-kaolin clay with different contents was completed on the II9220 automatic mercury intrusion porosimeter (pressure up to 400 MPa) using the MIP experimental method.

When preparing the mercury injection specimen, the middle of the cement specimen was selected for sampling, and the specimen was cut into small pieces of 3 mm~4 mm with scissors. Each sampling was used for at least two tests. After sampling, the hardened cement paste fragments should be immediately soaked in acetone to terminate the hydration and generally should be soaked for more than one day and night. Before the mercury injection test, the sample was taken out in the air to volatilize the acetone thoroughly and then placed in an oven at 105 °C to dry to constant weight to remove the moisture in the hole.

2.3.2. Calculation of Fractal Dimension

Many fractal models are available, including the Menger sponge model [30], the Zhang model [31], and the Neimark model [32]. These models have been used to analyze fractal features in concrete based on MIP data. One of the most widely used fractal models is Zhang's model, which uses the fractal dimension of the pore surface area [11,32,33] to analyze the pore structure in concrete. According to Zhang's model, the cumulative

intrusion work of mercury (W_n) and the total volume of mercury injected into the pore (V_n) follow a logarithmic law, which is shown as follows:

$$\ln \left(\frac{W_n}{\gamma_n^2} \right) = D_s \ln Q_n + \ln C \quad (1)$$

where γ_n (in m) denotes the minimum hole radius, C denotes the regression constant, and D_s denotes the fractal dimension of the hole surface. W_n is obtained from the following equation:

$$W_n = \sum_{i=1}^n p_i \Delta v_i \quad (2)$$

$$Q_n = \frac{V_n^{\frac{1}{3}}}{\gamma_n} \quad (3)$$

where p_i (in Pa) indicates the pressure at the i th mercury injection, v_i (in m^3) indicates the volume of mercury at the i th injection, and n is the total number of mercury pressings.

Scatterplot and linear regression analyses were performed using Origin. The linear regression equation and the correlation coefficient R^2 were calculated, and the slope of the linear regression equation was D_s , as shown in Figure 4. If the correlation coefficient is high, it indicates that the pore structure of the measured cement paste has obvious fractal characteristics.

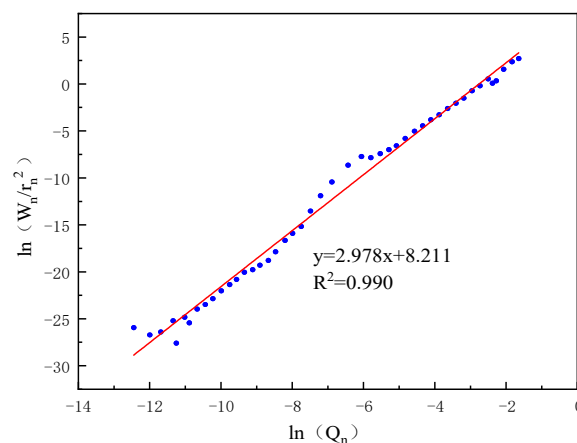


Figure 4. Fractal characteristics of pore structure of specimen NCH1 based on the thermodynamic model.

3. Results and Discussion

3.1. Pore Characteristics

In this test, the pore structure is analyzed for parameters such as pore size distribution, total specific pore volume, most probable pore size, average pore diameter, median pore diameter (volume) (the pore size when the pore volume is half of the total pore volume), and porosity. Different pore sizes can have different effects on the properties of cementitious materials. Academician Zhongwei Wu [34] classified the pore size of cementitious materials into four categories according to their influence: harmless pores ($d < 20$ nm), minimally harmful pores ($d = 20$ nm–50 nm), harmful pores ($d = 50$ nm–200 nm) and very harmful pores ($d > 200$ nm). For a more straightforward comparative analysis, this paper analyses the performance of nano-kaolinite clay in improving the pore structure of cement specimens according to this concrete pore structure classification method.

3.1.1. Total Specific Pore Volume and Most Probable Pore Size

The pore size distribution integral curve and pore size distribution differential curve characterizing the pore structure of cement were plotted using mercury intrusion test results, as shown in Figures 5 and 6.

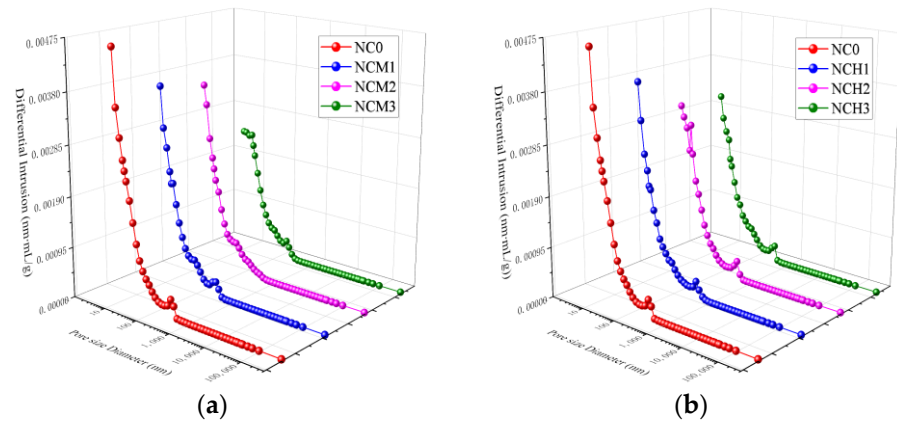


Figure 5. Integral curve of cement pore size distribution. (a) Mechanical dispersion; (b) manual dispersion.

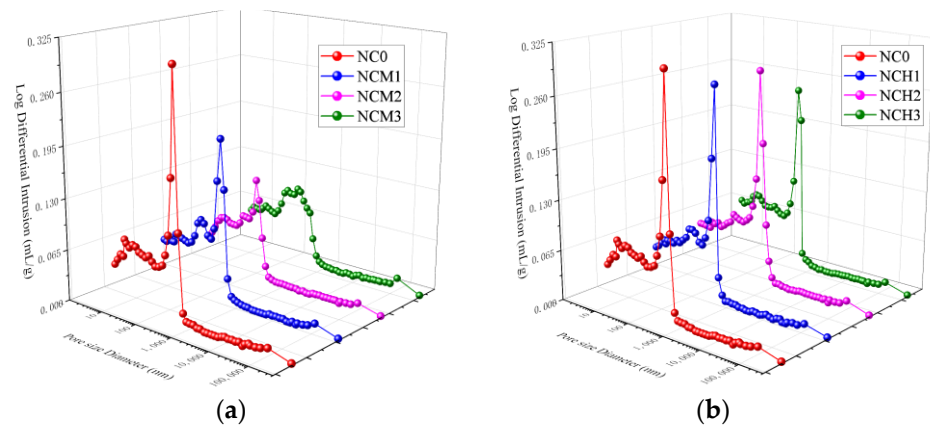


Figure 6. Differential curve of cement pore size distribution. (a) Mechanical dispersion; (b) manual dispersion.

The physical meaning associated with the peak of the integral curve of cement pore size distribution signifies the quantity of mercury absorbed into 1 g of the sample, also known as the total specific pore volume. As indicated in Figure 5, as the nano-kaolin content rises, the peak value on the integral curve of cement pore size distribution—whether through manual or mechanical dispersion—diminishes progressively. This translates to a descending trend in the total specific pore volume alongside the increase in nano-kaolin content. The physical interpretation of the peak on the differential curve of cement pore size distribution is that, in concrete, pore sizes smaller than this cannot form connected pore channels. It also represents the most probable pore size, which has the highest occurrence probability. As shown in Figure 6, this peak value decreases with increasing nano-kaolin content, indicating a gradual reduction in the most probable pore size. However, under manual dispersion, the impact of NCH1 and NCH2 is not significant.

Table 5 data reveal that adding NKC to the cement slurry significantly lowers the total specific pore volume. Compared to the control group, NCM1–NCM3 show decreases of 23.91%, 32.61%, and 47.83%, respectively. Similarly, the most probable pore size in the cement slurry with added NKC is reduced by 18.23%, 56.86%, and 56.87% compared to the control group. When manual dispersion is employed, NCH1, NCH2, and NCH3 demonstrate total specific pore volume reductions of 17.39%, 30.43%, and 32.61% compared to the control group.

Table 5. Total specific pore volume and most probable pore diameter of cement.

| Sample | Total Specific Pore Volume/mL/g | Percentage Increase/% | Most Probable Pore Size/nm | Percentage Increase /% |
|--------|---------------------------------|-----------------------|----------------------------|------------------------|
| NC0 | 0.0046 | 0.00 | 350.11 | 0.00 |
| NCM1 | 0.0035 | −23.91 | 283.97 | −18.89 |
| NCM2 | 0.0031 | −32.61 | 151.04 | −56.86 |
| NCM3 | 0.0024 | −47.83 | 151.01 | −56.87 |
| NCH1 | 0.0038 | −17.39 | 345.92 | −1.20 |
| NCH2 | 0.0032 | −30.43 | 340.81 | −2.66 |
| NCH3 | 0.0031 | −32.61 | 284.09 | −18.86 |

It can be seen that after mixing nano-kaolinite clay into cement, the nano-kaolinite clay particles promote the hydration reaction of cement and consume a large number of calcium hydroxide crystals to generate a large number of hydrated calcium silicate gel, which fills the tiny pores of the cement, thus making the pore structure of the cement more homogeneous and delicate and improving the denseness of the cement [5]. Notably, when the nano-kaolin clay content reaches 1.5%, the cement's improvement is most significant. A comparison between NCM and NCH specimens indicates that NCM has a greater reduction percentage in total specific pore volume compared to NCH, while NCM also exhibits a more significant reduction in the most probable pore size than NCH. This suggests that mechanical stirring enhances nano-kaolin clay particle dispersion, facilitating their entry into cement pores and thereby improving its pore structure.

3.1.2. Pore Size Distribution

According to Wu's [34] classification method of concrete pore structures, the pore structure of cement is divided into four pore size ranges, and the specific pore volume of each pore size range and its percentage in the total specific pore volume are compared. The detailed results are shown in Table 6. Figure 7 shows the histogram of pore size distribution.

Table 6. Pore size distribution of cement pastes.

| Sample | Pore Size Distribution/mL/g (%) | | | | Total Specific Pore Volume /mL/g |
|--------|---------------------------------|---------------------------------|---------------------------|------------------------------|----------------------------------|
| | Harmless Pores (<20 nm) | Little Harmful Pores (20–50 nm) | Harmful Pores (50–200 nm) | Much Harmful Pores (>200 nm) | |
| NC0 | 0.002971 (64.58) | 0.000802 (17.44) | 0.000566 (12.31) | 0.000261 (5.67) | 0.0046 |
| NCM1 | 0.002364 (67.57) | 0.000572 (16.35) | 0.000419 (11.97) | 0.000144 (4.11) | 0.0035 |
| NCM2 | 0.002139 (69.01) | 0.000528 (17.04) | 0.000311 (10.02) | 0.000122 (3.93) | 0.0031 |
| NCM3 | 0.001744 (72.69) | 0.000385 (16.05) | 0.000175 (7.31) | 0.000095 (3.95) | 0.0024 |
| NCH1 | 0.002518 (66.26) | 0.000617 (16.24) | 0.000455 (11.98) | 0.000209 (5.52) | 0.0038 |
| NCH2 | 0.002157 (67.42) | 0.000568 (17.76) | 0.000337 (10.55) | 0.000136 (4.27) | 0.0032 |
| NCH3 | 0.002137 (68.95) | 0.000552 (17.82) | 0.000264 (8.52) | 0.000146 (4.71) | 0.0031 |

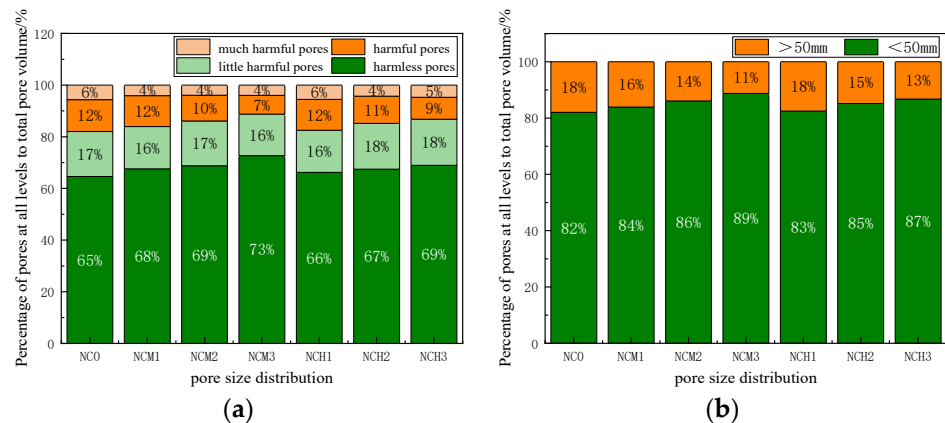


Figure 7. Percent of the specific pore volume of various grade pore sizes accounting for total specific pore volume. (a) Percentage of pore size (harmless pores, minimally harmful pores, harmful pores, very harmful pores); (b) percentage of pores size (>50 nm and <50 nm).

Table 6 and Figure 7 data reveal that as the nano-kaolin content rises, the proportion of harmless pores in the cement slurry correspondingly increases. Notably, NCM3 shows an 8% increase, while NCH3 demonstrates a 4% increase in comparison to the control group. By introducing nano-kaolin clay, the harmful and very harmful pores in cement decrease, while the harmless and minimally harmful pores increase. This adjustment in pore structure is a result of the nano-kaolin clay's ability to fill gaps between cement and stone materials, thereby reducing those gaps. Additionally, nano-kaolinite clay promotes the hydration reaction and generates more hydrated calcium silicate gels, which are adsorbent to the harmful substances in the cement, effectively degrading or stabilizing them [6,30].

Furthermore, the addition of nano-kaolin clay into cement not only reduces harmful and very harmful pores but also boosts the number of harmless and less harmful pores. This is because nano-kaolin clay effectively fills the small pores that are typically absent in cement materials, leading to a more uniform and detailed distribution of pores. Additionally, nano-kaolin clay enhances the bonding and cohesion of cement, enabling the formation of more harmless and less harmful pores. Consequently, incorporating nano-kaolin clay not only enhances the pore structure of cement but also enhances its mechanical properties and durability.

3.1.3. Porosity, Mean Pore Diameter, and Median Pore Diameter (Volume)

The cement's porosity, average pore diameter, and median pore diameter (volume) can also be obtained from the mercury pressure test. The specific test results are detailed in Table 7.

Table 7. Porosities, average diameters, and median diameters (volume) of cement.

| Sample | Porosity | | Average Hole Diameter | | Median Hole Diameter | |
|--------|------------|-----------------------|--------------------------|-----------------------|-------------------------|-----------------------|
| | Porosity/% | Percentage Increase/% | Average Hole Diameter/nm | Percentage Increase/% | Median Hole Diameter/nm | Percentage Increase/% |
| NC0 | 28.42 | 0 | 44.4 | 0 | 179.5 | 0 |
| NCM1 | 26.47 | −6.68 | 38.3 | −13.74 | 108.0 | −39.83 |
| NCM2 | 23.17 | −18.47 | 35.7 | −19.59 | 92.9 | −48.24 |
| NCM3 | 21.02 | −26.04 | 32.3 | −27.25 | 69.0 | −61.55 |
| NCH1 | 27.92 | −1.75 | 40.7 | −8.33 | 138.6 | −22.78 |
| NCH2 | 25.86 | −9.01 | 39.7 | −10.58 | 121.6 | −32.25 |
| NCH3 | 23.21 | −18.33 | 34.2 | −22.97 | 98.8 | −44.96 |

The mercury pressure test is a standard method of measuring porosity and pore size distribution. It calculates the sample's porosity and pore size distribution by placing it

under high pressure and allowing mercury to enter the open pores in the sample. However, since mercury can only enter the open pores in the structure, it cannot penetrate closed or non-open micro-gaps. Therefore, the porosity measured in the mercury intrusion test can only reflect the open, connected pores in the structure [34]. Therefore, the porosity in the test results does not reflect the total porosity of the structure, but only the porosity of the open pores, i.e., the apparent porosity.

In Table 7 and Figure 8a, it is evident that the porosity of NCM1, NCM2, and NCM3 decreased after the addition of nano-kaolin clay. This decrease was 6.68%, 18.47%, and 26.04% compared to the control group, respectively. This indicates that upon the addition of nano-kaolin clay, the original pore structure was either filled or altered, leading to a reduction in porosity. Notably, when the dosage was 1.5%, the porosity of cement significantly decreased. Similarly, the porosity of NCH1, NCH2, and NCH3 also decreased as the nano-kaolin content increased. The porosity of these materials was 1.75%, 9.01%, and 18.33% lower than the control group, respectively. A comparison between NCM and NCH reveals that the porosity of NCM is relatively smaller. Nanomaterials are agglomerated because of their very fine particles. The use of mechanical dispersion of nanomaterials is more adequate than artificial dispersion and is sufficient for more uniform mixing in water. Mechanical mixing ensures that nano-kaolinite clay particles are evenly distributed in cement, filling the larger pores effectively, thereby reducing the porosity of cement-based materials and enhancing the compactness of concrete.

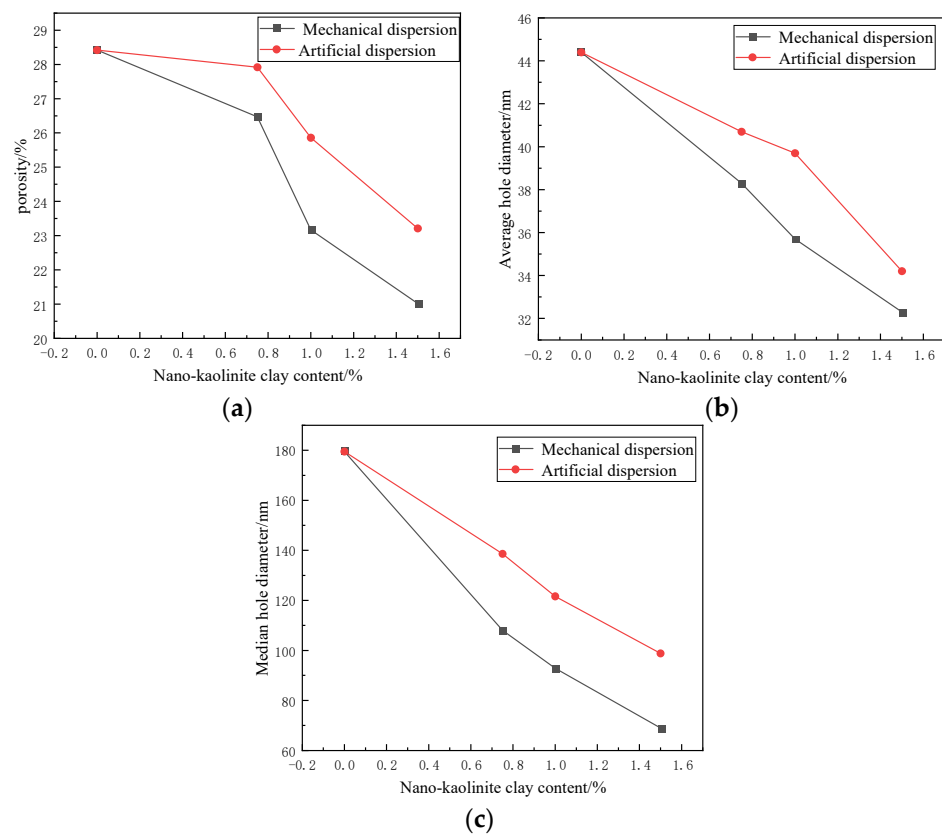


Figure 8. The relationship between nano-kaolinite clay content and pore structure of cement. (a) Porosity; (b) average pore diameter; (c) pore diameter (volume).

Table 7 and Figure 8b,c show that the incorporation of nano-kaolinite clay reduces the cement's average pore diameter and mesopore diameter. The reduction of NCM is significant, with the average and median pore diameter of NCM3 being reduced the most by 27.25% and 61.55%, respectively, compared to standard concrete. This indicates that the incorporation of nano-kaolinite clay can cause changes to the pore structure of the

cement, allowing the original pores to be filled or altered and, therefore, the pore diameter to become smaller, thus improving the properties and performance of the material.

3.2. Multifractal Dimension Discussion

3.2.1. Singularities

Figure 9 shows the thermodynamic fractal characteristics of the pore structure of the specimen NCH1 artificially dispersed as doped with 0.75% nano-kaolinite clay. Plotting the data computationally reveals an excellent linear relationship between the horizontal and vertical coordinates. However, there are some singularities in between, with the approximate pore diameter of the singularities ranging from L_1 to L_2 . Zeng et al. [35] also found a range of singularities in their study of the fractal characteristics of the pore structure of cement pastes. Zhang et al. [36] obtained similar results when studying the thermodynamic fractalization of building stones. For this case, the entire area can be divided into multiple ranges for multiple fractal comparisons to analyze the fractal characteristics more rationally. Therefore, the fractal characteristics were studied by dividing the aperture range into three intervals, I, II, and III, as shown in Figure 9 for the fractal study.

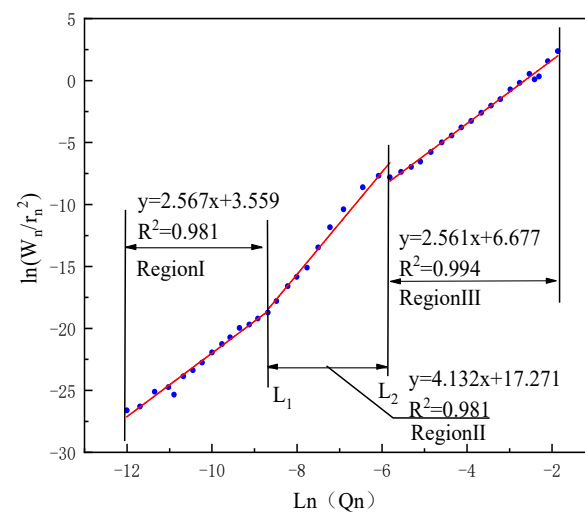


Figure 9. Fractal characteristics of the pore structure of NCH1.

In the analysis and establishment of microstructure and property relationships for cementitious materials, porosity (ϕ), critical pore diameter (d_c), and threshold pore diameter (d_{th}) can all reflect the pore structure characteristics of cementitious materials from different perspectives [37]. The critical pore diameter (as shown in Figure 10) is the diameter of the largest connected pore, which is the maximum pore size in the material through which a gas or liquid can flow and can reflect the material's permeability properties and pore structure characteristics. On the differential curve of pore size distribution, the critical pore size corresponds to the highest peak point on the curve [37]. The threshold pore diameter is the pore size distribution in which only a tiny amount of mercury can be pressed into the pore when it is greater than that size, and a large amount is required when it is less. It characterizes the largest connected pore size in the pore structure and relates to permeability properties [38]. The calculation of the threshold aperture is generally done using the point fitting method [37,38]. This is done by performing a linear fit to the cumulative distribution curve at data points significantly smaller and higher than the inflection point, obtaining two straight lines, and finding the pore diameter corresponding to their intersection point as the threshold aperture. The size of the threshold aperture diameter reflects the tightness of the material's pore structure and is essential for understanding properties, such as permeability, strength, and durability.

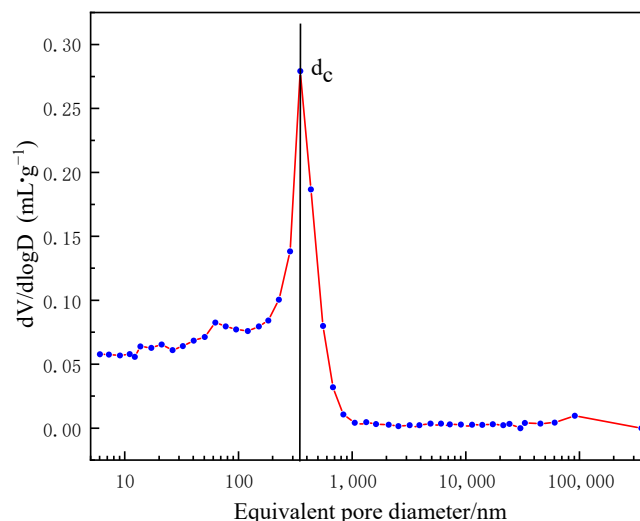


Figure 10. Critical pore size.

3.2.2. Multiple Fractal Features

The data in Table 8 show that the fractal dimension of the aperture range II ranges from 4.4 to 5.1. Mahyuddin et al. [17] showed that a power-law relationship for the fractal dimension of the pore surface area can be used to determine the fractal characteristics of a material, which should have a fractal dimension between 2 and 3. In contrast, when the pore structure was studied for nano-kaolinite clay cementitious materials, it was found that no fractal features were present in the pore size range II, which fell into the singularity range. In addition, Liu et al. [9] also used the Pfeifer model to conduct fractal research on the pore structure data of cement paste. In their study, the same phenomenon of zoning was found to exist. It is pointed out that the fractal dimension of the pore size range with sudden changes in pore volume is greater than three and does not possess fractal characteristics. In the application of fractal theory to study the pore structure of nano-kaolinite clay cementitious materials, it was found that the pore size range from 2 to 1000 nm possesses prominent fractal characteristics, and this result was also confirmed by many studies [37,38]. It is suggested that the sudden change in the amount of mercury pressure corresponds to a range of apertures that do not have fractal characteristics. This range is related to the threshold aperture.

Table 8. Fractal dimension and critical pore size of region II of nano-kaolinite clay cementitious materials.

| Sample | Ds | Critical Pore Diameter/nm |
|--------|---------|---------------------------|
| NC0 | 4.70327 | 349.9224 |
| NCH1 | 4.42734 | 340.1141 |
| NCH2 | 5.18094 | 284.0928 |
| NCH3 | 4.88805 | 151.0408 |
| NCM1 | 5.3928 | 345.8102 |
| NCM2 | 5.1641 | 283.9749 |
| NCM3 | 5.05763 | 161.0091 |

The fractal dimension of pore structure of nano-kaolinite clay cementitious material in pore size range I and III is shown in Figure 11. It can be concluded from that as the amount of nano-kaolinite clay increases, the fractal dimension of pore size range I decreases, while the fractal dimension of pore size range III increases. It is found that the increase in the number of micropores after adding nano-kaolinite clay leads to a small fractal dimension in pore size range I, indicating that the increased microporous structure is relatively simple. The decrease in the number of macropores after incorporation of nano-kaolinite clay is due to the fact that the hydration products generated from the hydration reaction of cement promoted

by the nano-kaolinite clay do not turn them into micropores after entering the large pores, but instead increase the complexity of the pore structure, thus leading to an increase in the fractal dimension in the pore diameter range III. Therefore, an increase in the amount of nano-kaolinite clay has a different effect on the fractal dimension of the pore structure.

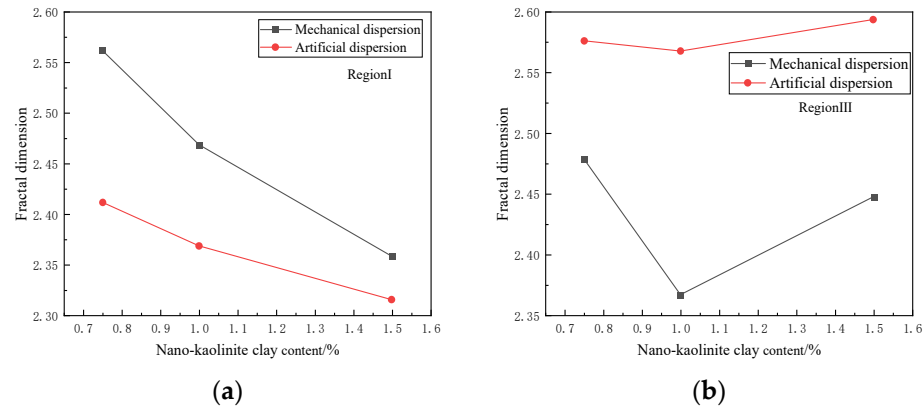


Figure 11. Fractal dimension of pore structure of nano-kaolinite clay cementitious material in the pore size range I and III. (a) Region I; (b) region III.

Compared to pore size range I, the nano-kaolinite clay has less influence on the fractal dimension of pore size range III. Pore size range I is mainly 5 to 1000 nm and comprises gel pores and small to medium-sized capillaries. The capillary pore is part of the space initially filled with water that was not filled with hydrates as the hydration reaction proceeded. The fractal dimension of the pore size range I should be related to the way and type of hydration products generated and more to the amount of nano-kaolinite clay. Therefore, the nano-kaolinite clay significantly influences the fractal dimension of the pore size range I.

On the contrary, the pore size range III is mainly greater than 2000 nm and composed of large capillary pores and pores. These pores are less affected by the change in the number of nano-kaolin clay pores than the pore size range I. It has been noted that this range's fractal dimension mainly reflects the particles' filling properties in the cement paste, which is related to the filling effect of nano-kaolinite clay [6,39,40]. The finer nano-kaolinite clay particles are filled between the voids of the cement particles to optimize particle build-up and improve the compactness of the cementitious material. This effect can reduce the fractal dimension of large capillary pores and stomata. The fractal dimension of the aperture range III increases with the increase in hydration age, which is consistent with the results in the literature. With the progress of hydration, the hydration products formed on the pore surface do not change the connectivity of large capillary pores and pores but increase the complexity of the surface and thus increase the fractal dimension [36]. It can be seen that the fractal dimension of the pore structure of nano-kaolinite clay cementitious materials in the different pore size ranges can be used to analyze the different effects of nano-kaolinite clay on the pore structure of cementitious materials.

3.2.3. Study on Permeability Based on Multifractal Features

The nature of the permeability of cement-based materials is the connectivity of pores, which is mainly influenced by capillaries pores and gel pores. The relationship between permeability and pore connectivity is well expressed by the Katz-Thompson model [41,42]:

$$k = cd_c^2 \frac{\sigma}{\sigma_0} \quad (4)$$

$$\frac{\sigma}{\sigma_0} = \frac{d_{\max}^e}{d_c} \phi S(d_{\max}^e) \quad (5)$$

where k is the permeability coefficient defined by the Darcy relationship; C is a constant, equal to $1/226$; d_c is the critical pore diameter; $\frac{\sigma}{\sigma_0}$ indicates the degree of connectivity of

the pore structure; d_{\max}^e is the conductivity characteristic size that produces the maximum conductivity, $d_{\max}^e = 0.68d_c$; ϕ is the porosity of the fractal range; and $S(d_{\max}^e)$ is the volume fraction of connected holes with an aperture larger than d_{\max}^e .

Tang et al. [43], based on fractal theory, derived an analytical expression for the fractal permeability coefficient (K) of porous materials based on the Hagen–Poiseuille equation and Darcy’s law:

$$K = \frac{(\pi D_f)^{\frac{1-D_T}{2}} [4(2-D_f)]^{\frac{1+D_T}{2}} \left(\frac{\phi}{1-\phi}\right)^{\frac{1+D_T}{2}} d_{\max}^2}{128(3+D_T-D_f)} \quad (6)$$

where D_f is the fractal dimension of the pore surface area, D_T is the fractal dimension of the hole curvature, and d_{\max} is the maximum aperture of the fractal range. Based on the assumption that the MIP pore is cylindrical, then $D_T = 1$ [43], and the fractal permeability coefficient K is expressed as follows:

$$K = \frac{2-D_f}{32(4-D_f)} \frac{\phi}{1-\phi} d_{\max}^2 \quad (7)$$

Many studies [44] have analyzed the relationship between the fractal dimension of cementitious materials and pore structure and properties for the entire range of pore sizes. This fractal approach calculates the fractal permeability coefficient using Equation (7). D_f and ϕ represent the fractal dimension and porosity of the entire pore size range, respectively. d_{\max} is the minimum pore size for which the cumulative pore volume is zero, and the calculation results are shown in Figure 12. The whole range of apertures contains the range of singularities. Also, according to Figure 11, it can be seen that different aperture ranges correspond to different fractal dimensions. The effect of nano-kaolinite clay on the fractal dimension of different pore sizes is also different. Therefore, the use of fractal dimensions over the entire pore size range does not give an accurate picture of the fractal characteristics of nano-kaolinite clay cementitious materials and is not conducive to the analysis of nano-kaolinite clay and the influence of the dispersion method. By analyzing Figure 12, it can be seen that the fractal dimension of the entire pore size range does not show a clear pattern with the nano-kaolinite clay content. Therefore, an appropriate range of pore sizes needs to be selected for analysis to more accurately characterize the fractal characteristics and properties of nano-kaolin clay cement-based materials. According to Figure 12, as the nano-kaolin content increases, the fractal permeability coefficient of the cement slurry exhibits a decreasing trend. This suggests that the inclusion of nano-kaolin effectively diminishes the permeability of the cement slurry, thereby enhancing its compactness. Furthermore, when mechanical dispersion is employed, the addition of nano-kaolin has a more significant impact on enhancing the pore structure of the slurry. Compared to manual dispersion, mechanical dispersion can more effectively improve the pore structure of cement slurry.

These findings indicate that the addition of nano-kaolin plays a crucial role in enhancing the performance of cement slurry. Reducing permeability and increasing compactness nano-kaolinite clay aids in improving the pore structure of the cement slurry, making it more robust and stable.

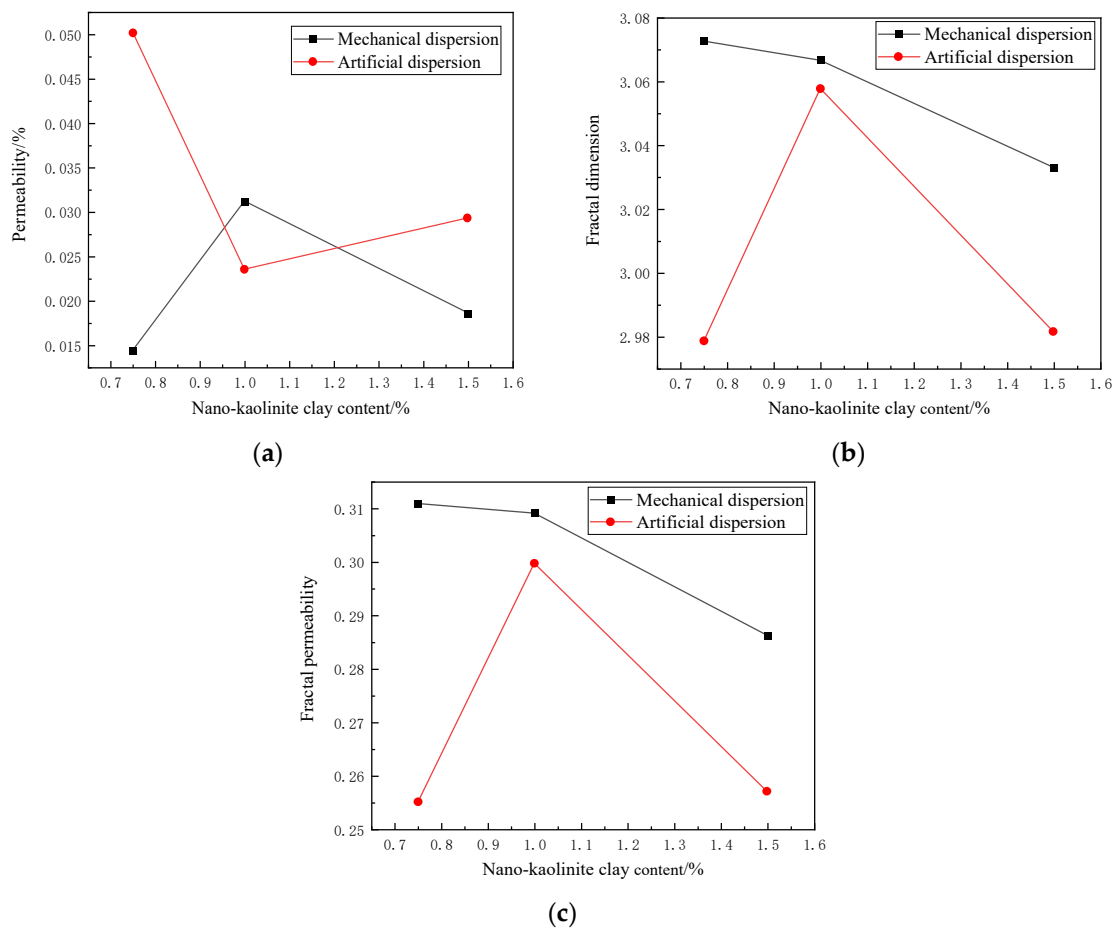


Figure 12. Fractal dimension of nano-kaolinite clay cement based on the whole pore size range. (a) Permeability; (b) the overall fractal dimension; (c) the fractal permeability coefficient.

The pore structure of nano-kaolinite clay cementitious materials has multiple fractal characteristics. Therefore, when calculating permeability based on fractal theory, pore size ranges that do not have fractal characteristics need to be circumvented, and fractal studies need to be conducted for pore size ranges relevant to permeability. Calculating the fractal permeability coefficient using Equation (7) requires using fractal dimensions and porosities smaller than the critical pore diameter range to be calculated. The results are shown in Figure 13.

By comparing Figures 13 and 11a, it can be seen that the range of pore sizes smaller than the critical pore diameter is closer to the pore size range I. The difference in fractal dimension between the two is negligible. At the same time, comparing the fractal permeability coefficients based on pore sizes smaller than the critical pore diameter range with those obtained based on the Katz-Thompson model shows good agreement between the two. Also, a good correlation between fractal dimension and permeability can be found in conjunction with Figure 14 for the range of pore sizes smaller than the critical pore diameter. This result further confirms that the correlation between fractal dimension and permeability is size dependent [38]. Therefore, the multi-fractal dimension can be used to characterize and calculate the permeability coefficient, which provides a theoretical basis for applying fractal theory to study, and analyze the actual permeability of cement-based materials.

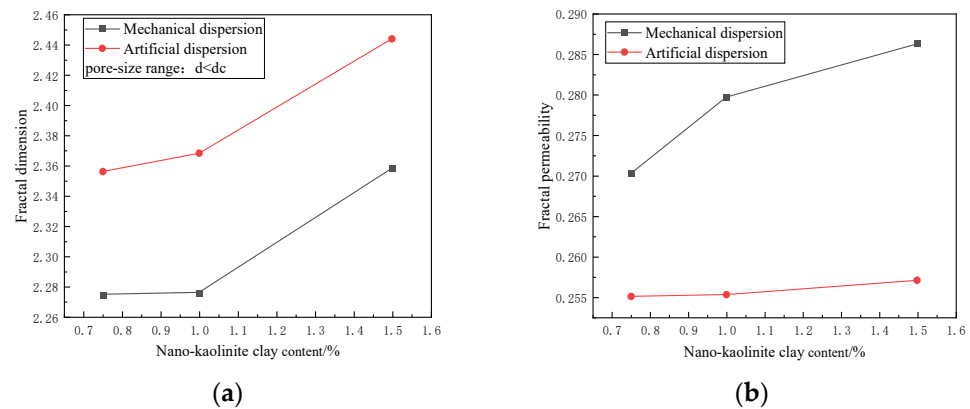


Figure 13. The fractal permeability coefficient of nano-kaolinite clay cementitious materials with a pore size less than the critical pore size range. (a) Fractal dimension; (b) fractal permeability.

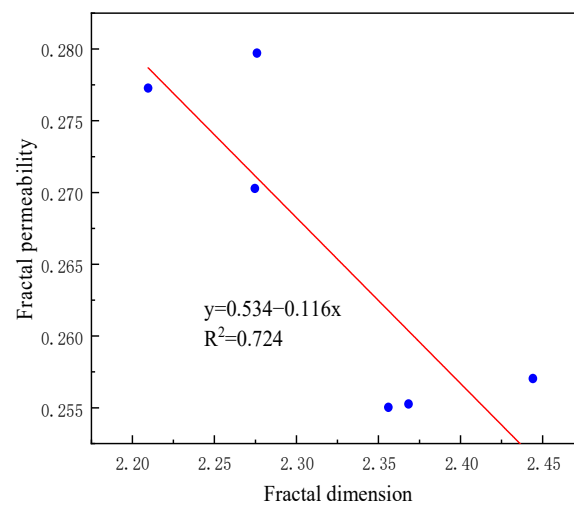


Figure 14. The relationship between fractal dimension (less than critical pore size) and fractal permeability.

In practical applications, the appropriate pore size range must be selected for fractal studies, considering the nano-kaolinite clay dosage and the specific application scenario. At the same time, attention must be paid to selecting the aperture range and the fractal calculation method's correctness to ensure the study results' accuracy and reliability. This will not only better reveal the relationship between nano-kaolinite clay and the pore structure and properties of cementitious materials but also provide theoretical support for practical engineering applications.

4. Conclusions

In order to improve the corrosion resistance of concrete at bridge piers, this paper describes the use of nano-kaolinite clay cement mortar. Combined with practical engineering applications, the main study is on high-performance mortars for surface treatment of piers and bridge columns, in which nano-kaolinite clay is incorporated to reduce the permeability of the surface of piers and bridge columns. In order to evaluate the anti-ionic erosion performance of nano-kaolinite clay cement mortar, we conducted detailed experiments on the pore structure of the cement paste. The following conclusions were obtained:

- (1) Adding nano-kaolinite clay particles improves the internal pore structure of the cement material. It shifts the pore size distribution toward the small pore size range, thus improving the compactness of the cement. Compared with the control group, the total specific pore volume and the most probable pore diameter of NCM3 decreased by 47.83% and 56.87%, respectively, and the harmful pores and very harmful pores

decreased the most. Thus, nano-kaolinite clay's improvement effect on cement pore structure is most pronounced at a doping level of 1.5%. It can reduce the total specific pore volume, most available pore size, porosity, median pore diameter (volume), and average pore diameter, thus refining the pore structure.

- (2) The fractal dimension image of nano-kaolinite clay cement-based material has a singular point range (pore size range II) and does not have fractal characteristics. The pore size distribution in this pore size range is different from that in other ranges. Aperture range I (smaller than aperture range II) and aperture range III (larger than aperture range II) have fractal characteristics. The pore size distribution in these two ranges adheres to the fractal law. The fractal dimension of pore size range I is more significant than that of pore size range III. These fractal features can be used to describe the pore structure of this material and help to investigate further and optimize the properties of the material.
- (3) The fractal dimension of pore size range I of cement paste is positively correlated with the content of nano-kaolinite clay, while the fractal dimension of pore size range III is negatively correlated with the content of nano-kaolinite clay. The effect of nano-kaolinite clay on the fractal dimension of pore size range I is more prominent.
- (4) The fractal dimension of the entire pore size range should not be used to analyze permeability but should be fractalized for the range smaller than the critical pore diameter. The obtained fractal dimension can effectively calculate the permeability coefficient. With the increase in nano-kaolinite clay content, the larger the fractal dimension is, the smaller the permeability coefficient is, and there is a good correlation between it and the permeability. The incorporation of nano-kaolinite clay has an important influence on the permeability of cement-based materials, and this effect can be effectively studied by fractal analysis.

Author Contributions: Writing-original draft, Funding acquisition, X.Y.; Methodology, H.L.; Resources, Formal analysis, Investigation, X.F.; Resources, Formal analysis, Investigation, L.Z.; Resources, Formal analysis, Investigation, C.Z.; Funding acquisition, Methodology, S.Z. All authors have read and agreed to the published version of the manuscript.

Funding: This research was funded by the Postdoctoral Program of Jiangsu Province in 2022 (grant number 2022ZB816) and the National Natural Science Foundation of China (grant number 51908342), to which the authors are very grateful.

Data Availability Statement: Data is contained within the article.

Acknowledgments: The authors gratefully acknowledge the support received from the funders.

Conflicts of Interest: Authors Xianzheng Yu, Xiaolin Fan, Liangyu Zhu and Chengqi Zhang were employed by the company China Railway Bridge and Tunnel Technology Co., Ltd. Author Hua Liu was employed by the company China Railway Major Bridge Reconnaissance & Design Institute Co., Ltd. The remaining author declares that the research was conducted in the absence of any commercial or financial relationships that could be construed as a potential conflict of interest.

References

1. Zhan, P.; He, Z.; Ma, Z.; Liang, C.; Zhang, X.; Abreham, A.A.; Shi, J. Utilization of nano-metakaolin in concrete: A review. *J. Build. Eng.* **2020**, *30*, 101259. [[CrossRef](#)]
2. Rishav, G.; Rajni, G.; Okon, E.N.; Amir, K.M.; Husain, K.A.; Thamer, A.; Parveen, B. Mechanical strength and durability analysis of mortars prepared with fly ash and nano-metakaolin. *Case Stud. Constr. Mat.* **2022**, *18*, E01796.
3. Manisha, V.; Parvez, A. Experimental study on metakaolin and nano alumina based concrete. *Mater. Today Proc.* **2022**, *11*, 296.
4. Ahmed, H.U.; Mohammed, A.S.; Faraj, R.H.; Abdalla, A.A.; Qaidi, S.M.; Sor, N.H.; Mohammed, A.A. Innovative modeling techniques including MEP, ANN and FQ to forecast the compressive strength of geopolymer concrete modified with nanoparticles. *Neural Comput. Appl.* **2023**, *35*, 12453–12479. [[CrossRef](#)]
5. Raheem, A.A.; Abdulwahab, R.; Kareem, M.A. Incorporation of metakaolin and nanosilica in blended cement mortar and concrete—A review. *J. Clean. Prod.* **2021**, *290*, 125852. [[CrossRef](#)]
6. Zhang, S.; Fan, Y.; Huang, J.; Surendra, P.S. Effect of nano-metakaolinite clay on the performance of cement-based materials at early curing age. *Constr. Build. Mater.* **2021**, *291*, 123107. [[CrossRef](#)]

7. Shilar, F.A.; Ganachari, S.V.; Patil, V.B. Advancement of nano-based construction materials—A review. *Constr. Build. Mater.* **2022**, *359*, 129535. [[CrossRef](#)]
8. Xie, J.; Zhang, H.; Duan, L.; Yang, Y.; Yan, J.; Shan, D.; Liu, X.; Pang, J.; Chen, Y.; Li, X.; et al. Effect of nano metakaolin on compressive strength of recycled concrete. *Constr. Build. Mater.* **2020**, *256*, 119393. [[CrossRef](#)]
9. Liu, K.; Wang, S.; Quan, X.; Duan, W.; Nan, Z.; Wei, T.; Xu, F.; Li, B. Study on the mechanical properties and microstructure of fiber reinforced metakaolin-based recycled aggregate concrete. *Constr. Build. Mater.* **2021**, *294*, 123554. [[CrossRef](#)]
10. Fan, Y.; Zhang, S.; Wang, Q.; Shah, S.P. The effects of nano-calcined kaolinite clay on cement mortar exposed to acid deposits. *Constr. Build. Mater.* **2016**, *102*, 486–495. [[CrossRef](#)]
11. Wang, L.; Luo, R.; Zhang, W.; Jin, M.; Tang, S. Effects of fineness and content of phosphorus slag on cement hydration, permeability, pore structure and fractal dimension of concrete. *Fractals* **2021**, *29*, 2140004. [[CrossRef](#)]
12. Hassaan, M.M.; Khater, H.M.; El-Mahllawy, M.S.; El Nagar, A.M. Production of geopolymer composites enhanced by nano-kaolin material. *J. Adv. Ceram.* **2015**, *4*, 245–252. [[CrossRef](#)]
13. Morsy, M.S. Behavior of blended cement mortars containing nano-metakaolin at elevated temperatures. *Constr. Build. Mater.* **2012**, *35*, 900–905. [[CrossRef](#)]
14. Mansi, A.; Sor, N.H.; Hilal, N.; Qaidi, S.M. The Impact of Nano Clay on Normal and High-Performance Concrete Characteristics: A Review. *Earth Environ. Sci.* **2022**, *961*, 012085. [[CrossRef](#)]
15. Zheng, X. Utilization of copper slag waste in alkali-activated metakaolin pervious concrete. *J. Build. Eng.* **2023**, *76*, 107246. [[CrossRef](#)]
16. Madandoust, R.; Mousavi, S.Y. Fresh and hardened properties of self-compacting concrete containing metakaolin. *Constr. Build. Mater.* **2012**, *35*, 752–760. [[CrossRef](#)]
17. Morsy, M.S.; Al-Salloum, Y.; Almusallam, T.; Abbas, H. Effect of nano-metakaolin addition on the hydration characteristics of fly ash blended cement mortar. *J. Therm. Anal. Calorim.* **2014**, *116*, 845–852. [[CrossRef](#)]
18. Ramli, M.B.; Alonge, O.R. Characterization of metakaolin and study on early age mechanical strength of hybrid cementitious composites. *Constr. Build. Mater.* **2016**, *121*, 599–611. [[CrossRef](#)]
19. Winslow, D.N. The fractal nature of the surface of cement paste. *Cem. Concr. Res.* **1985**, *15*, 817–824. [[CrossRef](#)]
20. Jin, S.; Zhang, J.; Chen, C. Study on fractal characteristics of pore structure of cement mortar. *J. Build. Mater.* **2011**, *14*, 92–97+105.
21. Han, X.; Feng, J.; Wang, B. Relationship between fractal feature and compressive strength of fly ash-cement composite cementitious materials. *Cem. Concr. Compos.* **2023**, *139*, 105052. [[CrossRef](#)]
22. Han, X.; Wang, B.; Feng, J. Relationship between fractal feature and compressive strength of concrete based on MIP. *Constr. Build. Mater.* **2022**, *322*, 126504. [[CrossRef](#)]
23. Qi, W.; Zhang, S.; Fang, Z.; Fan, Y.; Zheng, J. Effect of maintenance environment on the mechanical property and pore structure of cement paste mixed by seawater. *Constr. Build. Mater.* **2024**, *418*, 135280. [[CrossRef](#)]
24. Wang, S.; Gainey, L.; Mackinnon, I.D.; Xi, Y. High-and low-defect kaolinite for brick making: Comparisons of technological properties, phase evolution and microstructure. *Constr. Build. Mater.* **2023**, *366*, 130250. [[CrossRef](#)]
25. Liu, K.; Ostadhassan, M.; Kong, L. Multifractal characteristics of Longmaxi Shale pore structures by N₂ adsorption: A model comparison. *J. Petrol. Sci. Eng.* **2018**, *168*, 330–341. [[CrossRef](#)]
26. Valentini, L.; Artioli, G.; Voltolini, M.; Dalconi, M.C. Multifractal analysis of calcium silicate hydrate (C–S–H) mapped by X-ray diffraction microtomography. *J. Am. Ceram. Soc.* **2012**, *95*, 2647–2652. [[CrossRef](#)]
27. Lange, D.A.; Jennings, H.M.; Shah, S.P. Image analysis techniques for characterization of pore structure of cement-based materials. *Cem. Concr. Res.* **1994**, *24*, 841–853. [[CrossRef](#)]
28. Liu, Y.; Deng, H. Study on permeability performance of cemented tailings backfill based on fractal characteristics of pore structure. *Constr. Build. Mater.* **2022**, *365*, 130035. [[CrossRef](#)]
29. Mendoza, F.; Verboven, P.; Ho, Q.T.; Kerckhofs, G.; Wevers, M.; Nicolai, B. Multifractal properties of pore-size distribution in apple tissue using X-ray imaging. *J. Food Eng.* **2010**, *99*, 206–215. [[CrossRef](#)]
30. Jiyoung, K.; Geuntae, H.; Sangwoo, O.; Seongcheol, C. Application of various fractal models in characterizing the morphology of pore structures of hydrating cement pastes. *J. Mater. Res. Technol.* **2022**, *20*, 3818–3835.
31. Zhang, B.; Li, S. Determination of the Surface Fractal Dimension for Porous Media by Mercury Porosimetry. *Ind. Eng. Chem. Res.* **2002**, *34*, 546–557. [[CrossRef](#)]
32. Neimark, A. A new approach to the determination of the surface fractal dimension of porous solids. *Phys. A Stat. Mech. Its Appl.* **1992**, *191*, 258–262. [[CrossRef](#)]
33. Zhang, L.; Zhou, J. Fractal characteristics of pore structure of hardened cement paste prepared by pressurized compact molding. *Constr. Build. Mater.* **2020**, *259*, 119856. [[CrossRef](#)]
34. Liu, P.; Cui, S.; Li, Z.; Xu, X.; Guo, C. Influence of surrounding rock temperature on mechanical property and pore structure of concrete for shotcrete use in a hot-dry environment of high-temperature geothermal tunnel. *Constr. Build. Mater.* **2019**, *207*, 329–337. [[CrossRef](#)]
35. Wu, Z.; Lian, H. High performance concrete. *CRExpress* **1999**, *43*, 73–95.
36. Zeng, Q.; Luo, M.; Pang, X.; Li, L.; Li, K. Surface fractal dimension: An indicator to characterize the microstructure of cement-based porous materials. *Appl. Surf. Sci.* **2013**, *282*, 302–307. [[CrossRef](#)]

37. Zhang, B.; Liu, W.; Liu, X. Scale-dependent nature of the surface fractal dimension for bi- and multi-disperse porous solids by mercury porosimetry. *Appl. Surf. Sci.* **2006**, *253*, 1349–1355. [[CrossRef](#)]
38. Ma, H. Mercury intrusion porosimetry in concrete technology: Tips in measurement, pore structure parameter acquisition and application. *J. Porous Mater.* **2014**, *21*, 207–215. [[CrossRef](#)]
39. Liu, Z.; Winslow, D. Sub-distributions of pore size: A new approach to correlate pore structure with permeability. *Cem. Concr. Res.* **1955**, *25*, 769–778. [[CrossRef](#)]
40. Fan, Y.; Zhang, S.; Kawashima, S.; Shah, S.P. Influence of kaolinite clay on the chloride diffusion property of cement-based materials. *Cem. Concr. Compos.* **2014**, *45*, 117–124. [[CrossRef](#)]
41. Wang, D.; Shi, C.; Farzadnia, N.; Shi, Z.; Jia, H.; Ou, Z. A review on use of limestone powder in cement-based materials: Mechanism, hydration and microstructures. *Constr. Build. Mater.* **2018**, *181*, 659–672. [[CrossRef](#)]
42. Katz, A.J.; Thompson, A.H. Quantitative prediction of permeability in porous rock. *Phys. Rev. B* **1986**, *34*, 8179. [[CrossRef](#)] [[PubMed](#)]
43. Katz, A.J.; Thompson, A.H. Thompson. Prediction of rock electrical conductivity from mercury injection measurements. *J. Geophys. Res. Solid Earth* **1987**, *92*, 599–607. [[CrossRef](#)]
44. Tang, S.; He, Z.; Cai, X.; Cai, R.; Zhou, W.; Li, Z.; Shao, H.; Wu, T.; Chen, E. Volume and surface fractal dimensions of pore structure by NAD and LT-DSC in calcium sulfoaluminate cement pastes. *Constr. Build. Mater.* **2017**, *143*, 395–418. [[CrossRef](#)]

Disclaimer/Publisher’s Note: The statements, opinions and data contained in all publications are solely those of the individual author(s) and contributor(s) and not of MDPI and/or the editor(s). MDPI and/or the editor(s) disclaim responsibility for any injury to people or property resulting from any ideas, methods, instructions or products referred to in the content.